INTRODUCTION TO HIGH *PT* PHYSICS AT THE TEVATRON

H.J. FRISCH
Physics Dept. and Enrico Fermi Inst.
Univ. of Chicago, IL 60637

Abstract. A pedagogical treatment of high p_T physics at the Tevatron, including recent searches for SUSY and precision measurements of the W boson and top quark masses is given in two lectures. The intended audience is young theorists, and the lectures are intended to be an introduction to the experimental problems and techniques unique to a hadron collider, concluding with the present status of selected results from CDF and DØ.

1. Introduction

The goals of these lectures are to teach an audience largely composed of young theorists enough of the jargon and the basic issues to enable them to appreciate other, better, talks than these, and, to help develop a critical eye for experimental aspects of making measurements at a hadron collider. An apology to my DØ colleagues is in order: I know more about CDF than DØ, and so there is more detail about techniques from CDF. In addition, I have focussed on a few favorite topics to give the flavor of the work rather than try to give a survey of all the results. The lectures had many figures, far too many for this writeup; I have omitted the discussions of some of the SUSY channels, the SUSY Higgs sector, including the charged Higgs searches (a long story in itself), and much of the details of the top quark and W boson mass measurements. I've tried, however, to select references to elucidate details. For a comprehensive survey of the SUSY searches the reader is encouraged to read Refs. [1, 2]. Lastly, after the lectures were given many numbers changed in later conferences; for consistency I have left the figures and numbers as they were when the lectures were given. The new Tevatron figures and numbers can be found from the web pages in the references.

2. The Tevatron $\bar{p}p$ Collider

The Tevatron is a 1-km radius superconducting accelerator ring at Fermilab, with a current top operating energy of 900 GeV. The Main Ring is (was[3]) the original 400 GeV non-superconducting machine in the same tunnel; it was used to make anti-protons by extracting the beam at 150 GeV onto an external target. Negative particles were then collected by a strong magnetic 'lens' downstream of the target, and the anti-protons stored in a double set of storage rings. Both rings employ stochastic cooling: the Debuncher ring to collect and cool each initial pulse of antiprotons; subsequently antiprotons are transferred to the Accumulator ring where they are stored over a long period as the beam of antiprotons is condensed in phase space. Anti-protons are then extracted from the core of the 'stack' (the densest part of phase-space), accelerated in the Booster and injected first into the Main Ring and then the Tevatron, but travelling in the counter-rotating direction from protons. Protons are then accelerated through the complex and injected into the Tevatron. The Tevatron is then ramped up in energy to 900 GeV. The final set of steps consists of 'coalescing' the many bunches of protons and antiprotons into 6 bunches of each (still counter-rotating), and then 'squeezing' the beams into a tight focus at the center of the two interaction regions B0 (where CDF is located), and DØ, where the eponymous DØ experiment is (the Tevatron has 6-fold symmetry, with the centers of the straight-sections labelled A0, B0, etc.).

The properties of the Tevatron Collider for Run Ib (1994-5) and the upcoming Run II (presently scheduled for Spring of 2000) are given in Table 2 [4].

A key property is the luminosity, which is simply the coefficient that gives the proportionality between the rate for a process and its cross-section:

$$\text{Rate (events/sec)} = \mathcal{L}\ (\text{cm}^{-2}\text{s}^{-1}) \times \text{cross-section (cm}^2) \ ;$$

Integrated luminosity is a measure of the total number of proton-antiproton collisions, and is just the time-integral of luminosity:

$$\text{Total number of events accumulated} = \int \mathcal{L}dt\ (\text{cm}^{-2}) \times \text{cross-section (cm}^2)\ .$$

For example, CDF and DØ each have an integrated luminosity $\int \mathcal{L}dt \approx 100$ pb^{-1}, so with a top pair cross-section of 5 pb, we expect 500 top pairs (5 $pb \times 100\ pb^{-1}$). Some easily remembered other benchmarks are that the cross-section times branching ratio for $W^{\pm} \rightarrow e^{\pm}\nu$ is about 2 nb (2000 pb), and for $Z^0 \rightarrow e^+e^-$ is approximately 1/10 of that (200 pb). The total $\bar{p}p$ cross-section is approximately 75 mb (75×10^{-27} cm$^{-2}s^{-1} = 75 \times 10^9$ pb).

TABLE 1. Typical properties of the Tevatron Collider for Run Ib, and projected for the upcoming Run II.

	Run Ib	Run II	Units
Number of Bunches	6	36 ($\rightarrow$ 121 ?)	
Bunch Spacing	3500	396 ($\rightarrow$ 132?)	nsec
Protons/bunch	2.3	2.7-3.3	10^{11}
Anti-protons/bunch	0.55	0.55	10^{11}
Total Antiprotons	3.3	20	10^{11}
Beam Energy	900	1000	GeV
Typical Luminosity	1.6	20	10^{31} cm^{-2}s^{-1}
Interactions/Crossing	2.5	5.3 ($\rightarrow$ 1.8?)	
Integrated Luminosity	3.2	41	pb^{-1}/week

3. Problems Unique to Working at a Hadron Collider

There are a number of problems that are unique to hadron colliders; some are unique to the Tevatron and $\bar{p}p$, but most are inherent and will be present at the LHC.

The Trigger Problem. From the above cross-section and luminosity numbers one can easily see that there is a serious problem with event rates and the capability of recording and handling data. A luminosity of 10^{32} (and this is only 1% of the LHC design luminosity) corresponds to ≈ 5 MHz of inelastic collisions. An event in CDF contains about 1/4 Megabyte of data[5], and so if each event were recorded in full the datastream corresponds to approximately 1 Terabyte per second. However only a small fraction of these events contains the high-momentum-transfer physics we want to explore. Figure 1 shows the cross-sections for various processes of interest. The trigger problem consists of maintaining a high and known efficiency for those events one wants while rejecting unwanted events at a very high rejection factor and rate.

Energy Calibration. Because the parton-parton interactions have a wide range of energies, the beam energy provides no energy scale calibration, unlike at LEP. Normalization of the energy calibration of the detector has to come from both test-beam data and *in situ* data. Long experience has taught us that the *in situ* calibrations are critical, and a number of techniques have been developed. CDF has a magnetic spectrometer in front of its calorimeters, and uses the J/ψ, Υ, and Z^0 peaks to calibrate (although

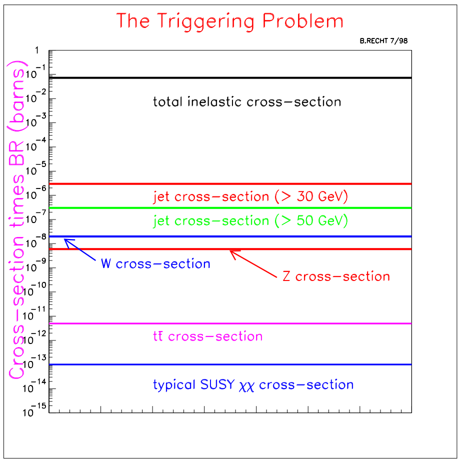

Figure 1. The triggering problem: selecting the most interesting physics at high efficiency with typical rejecting factors of 10^6.

the absolute calibration using NMR and the field is highly accurate as well); DØ does not have a magnetic spectrometer, and uses the π^0 (!), J/ψ, and Z^0 peaks[6].

The normalization of the hadron calorimeters for measurement of jet energy spectra is more difficult. Calibration of the energy scale is made by balancing the transverse momentum of jets against that of photons or $Z^0 \rightarrow e^+e^-$ decays. The W and Z bosons in principle should be good sources of dijet events for calibration via reconstructing the mass. However the rate for two jets from QCD processes is so large that at the Tevatron these events are not easily seen, and the triggers have to be 'prescaled'- i.e. only a small fraction of them are accepted. Also the transverse energies of the jets from the W and Z are close to the trigger threshold, where efficiencies are rapidly changing. Because of these difficulties, the W and Z so far have not been useful as a calibration of the jet energy scale. In Run 2, the top quark will provide several hundred events with W decays to two jets for calibration. The advent of triggers that can identify b-decays by displaced vertices in the next run may also help the situation, at least for b-jets.

Multiple Interactions/Crossing. The crossing rate of proton and antiproton bunches at the Tevatron is 286 KHz with 6 bunches. At the peak luminosity of Run I of about 2×10^{31} there are on order 1 MHz of collisions, and so approximately 3-4 collisions per crossing (not all bunches of either protons or anti-protons have the same number of particles). While most of these collisions are 'soft' (small momentum-transfer), they produce extra particles and add to the 'underlying event'. The average energy in a tower of the calorimeter is seen to depend on the number of collisions, for example, as does the density of hits in the tracking chambers.

Extended Luminous Region. This is both good news and bad news: the bunches in the Tevatron have a typical length of $\approx$ 1 m; the convolution of two bunches results in a distribution of the event vertex along the beam direction ('z' in most detector coordinate systems) with an rms of 30 cm. The good news is that this allows the tracking systems to resolve individual vertices much of the time (typical resolutions in z are several mm in Run I); the bad news is that calculating transverse energies involves the sine of the angle between the beamline and a line running from the vertex to the deposition of energy, and consequently confusion as to the correct vertex results in mismeasured transverse energies. In addition, a line-source makes acceptance issues more complicated, as the detector response depends on both the angle of incidence and the position of the energy deposited.

Normalizing Cross Sections. If the beam sizes and fluxes were precisely known one could calculate cross-sections for the production of different processes from first principles. Traditionally cross-sections are normalized to the total $\bar{p}p$ cross-section. However this is a very difficult measurement, and the results from several experiments are inconsistent[7]. It may make sense to normalize all cross-sections to the W cross-section, for example, as it has a distinctive and easily measured signature, and is directly related to the processes used to generate the theoretical parton-distribution functions used to compare experimental measurements to predictions[8]. (This is an idea whose time hasn't yet come, but will.)

4. Flavor Identification (Hadrons and Leptons)

Perhaps the biggest surprise has been how well we can identify flavor, and how much power we have to determine specific signatures involving flavor. (CDF stands for 'Collider Flavor Detector'?). Similarly, we knew we could identify electrons and muons, but did not take tau identification seriously. Below we briefly discuss how each of these 'objects' is identified:

Electrons. An electron will shower in the lead (CDF) or uranium (DØ) electromagnetic calorimeter. The shower is narrow and has a well-defined shape both longitudinally and transversely[9]. A track has to point to the shower; in CDF the momentum of the track (p) has to match the energy of the shower (E). More detail can be found in Ref. [10, 11], as well as papers in the same areas on W and Z production.

Muons. A muon will penetrate both the electromagnetic and hadronic calorimeters and will leave a track in the muon chambers behind. A track in the tracking chambers is required to match the track in the muon chambers, in general. A muon typically deposits a few hundred MeV in an electromagnetic calorimeter and several GeV in a hadronic calorimeter; a high-

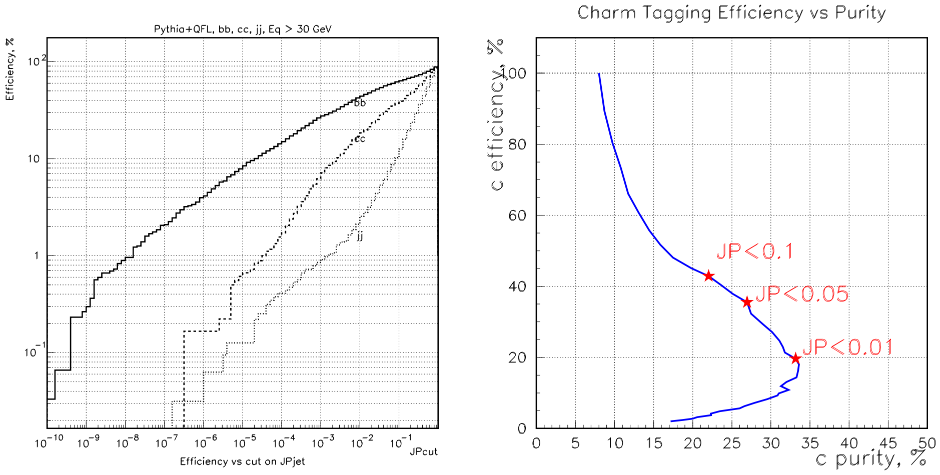

Figure 2. Left: The frequency distribution in the CDF variable JETPROB, which is the probability that a jet comes from the primary vertex, for light quarks and gluons (top curve), charm (middle curve), and bottom (bottom curve). A cut at 1%, for example, enhances heavy flavor over light quarks. Right: The efficiency versus purity curve for charm identification, with three values of the JETPROB cut identified.

momentum charged track that leaves much less energy than its measured momentum is also classified as a muon by CDF (which has less muon coverage than DØ). For more detail, see Ref. [10, 11].

Taus. Taus decay primarily into one or three charged pions, with accompanying π^0s. A high-momentum single track or triad of tracks, 'isolated' in that there is little energy in the calorimeter around the tau-candidate cluster, and no other tracks nearby, is the signature of a hadronically decaying tau. Tau's can be separated from the jet backgrounds in samples that have other factors that discriminate against QCD jets. In some cases one can detect the displaced vertex of the tau decay. For a study of tau detection in top events see Ref. [12].

Neutrinos. Neutrinos (and neutralinos too, perhaps?) are (obviously) not directly detected, but can be inferred by an imbalance in total transverse momentum in an event. For details of how these are measured, see Ref [11, 13].

Light Quarks and Gluons. These appear as jets, and are not differentiated as to quark or gluon origin in any analyses other than a few QCD analyses, in general. Both CDF and DØ identify jets by using a cone algorithm to cluster energy in the eta-phi space of calorimeter energy (the radius in $\eta - \phi$ space, R, is 0.5 for DØ and 0.4 for CDF for top analyses, for example) [10, 14].

Charm Quarks. A new development is the ability of CDF to 'tag' (identify as a candidate) inclusive decays of charm quarks through the displaced

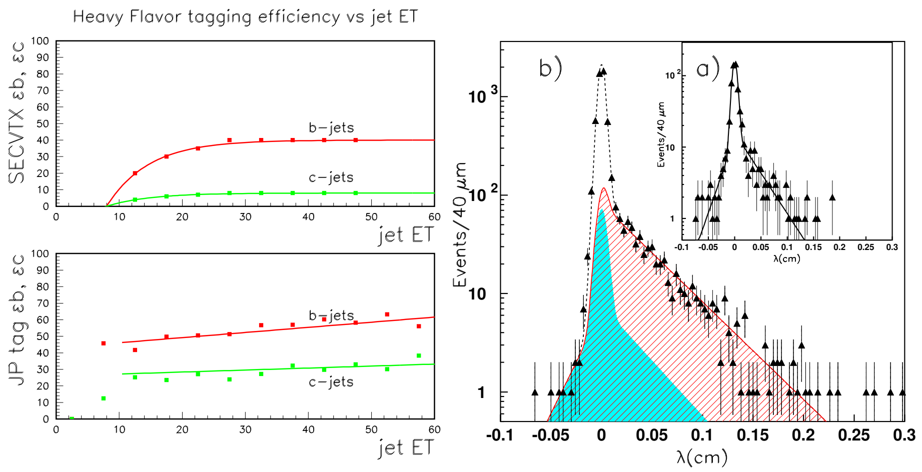

Figure 3. Left: The CDF tagging efficiency for charm and bottom quarks for the algorithm used in the top search (top plot) and JETPROB (lower plot). Right: The b-lifetime as measured by CDF. The inset shows the sidebands in mass.

vertex resulting from the charm lifetime and also the differences in fragmentation from bottom quarks[15]. Figure 2a shows the distributions in the variable 'Jet Probability', which is the probability that a track comes from the beam line (as opposed to coming from a point displaced off the beam) for light quark and gluon jets, charm, and bottom. Figure 2b plots the efficiency for identifying charm versus the purity, with the points in the space identified for a cut on Jet Probability of 10%, 5%, and 1%.

Bottom Quarks. Bottom quarks are tagged both by the displaced vertex (CDF) and by leptons from the semi-leptonic decays (CDF and DØ). Figure 3a shows the efficiencies measured by CDF for a vertex-finding algorithm (SECVTX) and also the Jet Probability algorithm which looks for tracks that do not point back to the beam line. The lifetime of hadrons containing b-quarks is shown in Figure 3b. The tagging algorithms are described in detail in the papers on the top discovery[10, 11].

Top Quarks. The top quark[10, 11] has been observed in the channels $t \to Wb$, $W \to jj$, $W \to e\nu$ or $\mu\nu$, and (with only a few events) $W \to \tau\nu$. However, because the top quark is produced in $t\bar{t}$ pairs, the channels are described by the decay products of the pair: 'lepton+jets', 'dilepton', 'all-hadronic', and 'tau-dilepton'. The measurement of the top mass is described in a section below; it is a good example of kinematic reconstruction of the mass and decay modes of a heavy object, of the kind that is necessary in searching for new heavy states such as in SUSY.

Photons. The signature of a photon is like that of an electron, but without a track in the tracking chambers[16, 20]. It has a narrow cluster of energy in the electromagnetic calorimeter, with little leakage into the hadronic calorimeter behind. The dominant background to direct photon production is pairs of real photons from π^0 and η mesons, which are copiously produced in jets. The probability that a jet 'fakes' an isolated photon is on the order of 10^{-3}. In CDF, the measurement of the shower profile can discriminate the two photons from a π^0 from a single photon up to transverse momenta of $\approx$ 30 GeV; above that one can distinguish the two cases on a statistical basis by the fraction of photon candidates that convert (make e^+e^- pairs) in the 1-radiation length of the magnet coil in front of the calorimeter. Lastly, at much reduced efficiency, with CDF one can look for conversions in the spectrometer material itself: this allows pointing the photon back to its source; DØ can use the multiple sampling in depth in the electromagnetic calorimeter to achieve some pointing capability.

W Bosons. The W has been reconstructed in the $e\nu$, $\mu\nu$, and $\tau\nu$ modes at the Tevatron, and, in top decay, in the jet-jet mode (the W mass is too low to allow triggering on the $W \to jj$ mode at reasonable efficiency at the Tevatron). More details are given in the section on the precision measurement of the W mass below.

Z Bosons. The Z cross-section is about 1/3 that of the W, and the leptonic decays are down by another factor of 3, so the number of $Z^0 \to e^+e^-$ decays is approximately 1/10 that of $W^\pm \to e^\pm\nu$ decays. As in the W case, $Z \to jj$ has been below trigger threshold (except in the case of $Z^0 \to b\bar{b}$, where the trigger is on a muon from the decay of one of the b's). The Z serves as an important normalization in measurements of the property of heavy particles such as the W and top, as well as a clean source of leptons for efficiency measurements.

4.1. SOME SUBTLETIES

It seems obvious to experimentalists that the identification of some set of numbers in the data as corresponding to an 'electron' or a 'muon' means that these are candidates, with some finite probability that they are background instead. Estimating and/or measuring the 'fake rates' and the efficiencies for the identification of objects is a major part of looking for new signatures. The fake rates are detector-dependent and sample-dependent; in a hadron collider one selects samples out of a much larger pool of events. As a specific example of the problem, consider muon identification in CDF. A 'muon' is defined as a track that matches a track ('stub') in the muon chambers, and (in many analyses) that leaves less than 2 GeV in the electromagnetic calorimeter and less than 6 GeV in the hadronic. Consider what happens if the muon radiates a co-linear photon: if the bremsstrahlung is very hard (i.e carries a way most of the muon momentum), the muon track will bend away from the photon calorimeter cluster, and the muon will be identified as a photon. If the track points within a few mm of the cluster, the muon will be called an electron, although (in general) the ratio of E (calorimeter) to p (track) will not be right. And, if the muon is in the same tower(s) as the photon, but doesn't point at the cluster, the electromagnetic energy will disqualify the track as a muon, and the no-track requirement will disqualify the cluster as a photon, and the object just vanishes (the momentum isn't counted anywhere). Electron, photon, and jet identification have similar subtleties. *Caveat emptor.*

5. Measuring the W Boson Mass

The precise measurement of the W mass is difficult: one is reconstructing the energy of an object with a finite width ($\approx$ 2.2 GeV) that decays into a charged lepton and a neutrino that is not measured, to a level of $\approx$ 0.1% (80 MeV). Moreover, the W is produced with substantial momentum both along the beam direction and transverse to it, The quantities measured are the lepton momentum/energy, and the transverse momentum of the particles produced along with the W that recoil against the p_T of the W (these include initial and final state radiation from the partons and particles).

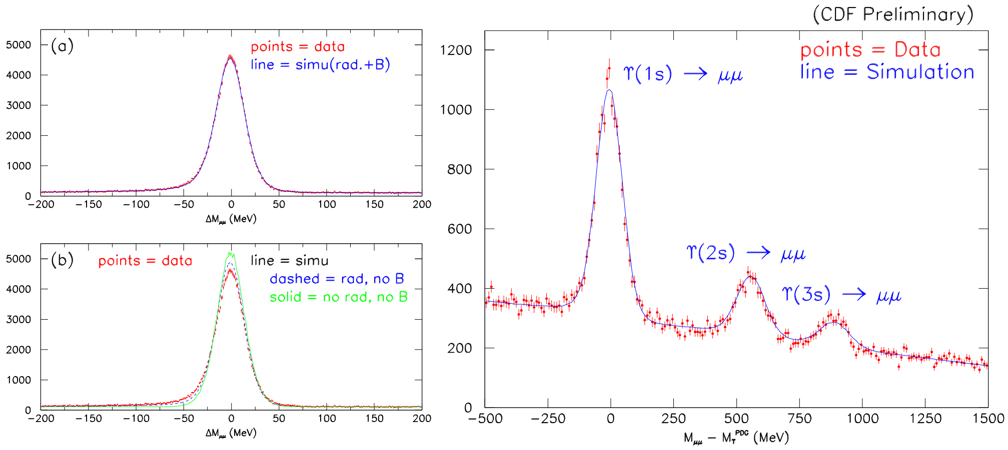

Figure 4. The dimuon states used to normalize the CDF momentum scale. Left: The dimuon distribution in the region of the J/ψ mass, compared to Monte Carlo with and without radiative corrections; Right: The dimuon distribution in the region of the Υ mass.

I describe here the preliminary CDF $W^\pm \to \mu^\pm \nu$ measurement as an example: in this case the strategy is to normalize the mass scale to the J/ψ, and check with the Υ and the Z. There are alternative strategies: DØ, which uses its calorimeter to measure the $W^\pm \to e^\pm \nu$ mode, normalizes to the Z, for example. The CDF analysis of the Run 1b data first sets the

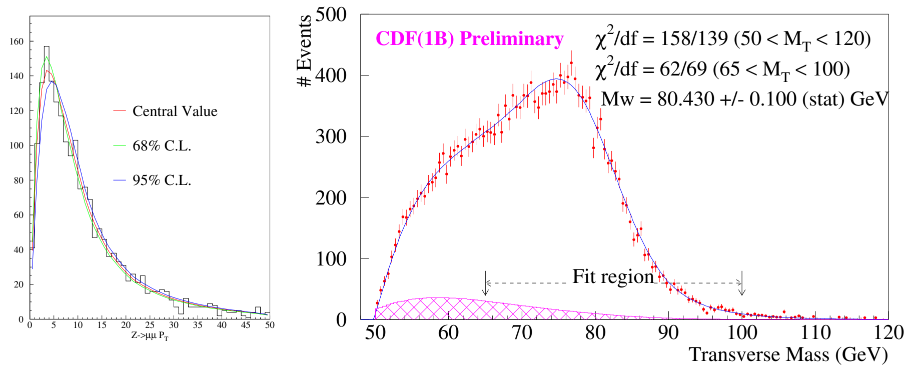

Figure 5. Left: The measured and fitted p_T spectra from $Z^0 \rightarrow \mu^+\mu^-$ decays in CDF, used to model the W p_T spectrum; Right: The final transverse mass plot comparing data and the final fit for the W mass.

momentum scale from the J/ψ mass spectrum, shown in Figure 4a. The J/ψ mass is measured to be 3096.2 ± 1.1 MeV, with the uncertainty dominated by energy loss in the material of the spectrometer before the track is measured in the outer tracking chamber. Comparing this to the world average generates a correction factor for the momentum scale of 1.00023 $\pm$ 0.00048; including the uncertainty on the extrapolation to the curvature characteristic of muons from W decay generates a total uncertainty on the W mass of 40 MeV. The upsilon mass, shown in Figure 4b, is used to check the momentum scale.

6. Measuring the Top Quark Mass

The measurement of the top mass has been made in the lepton+jets channel[21, 22], the dilepton channel[23, 24], and the all hadronic channel (6-jets)[25]. The measurement in the lepton+jets channel is done by a constrained fit of the invariant mass of the top and the antitop to the hypothesis $t \rightarrow Wb$; one t results in 3 jets (one of which is a b-quark), and so is fully reconstructed; the other gives lepton+neutrino+b-quark. This results in a 1C (one constraint) fit. In the dilepton channel both W's decay leptonically, and because there are two neutrinos there are fewer constraints than measured quantities. In this case probabilistic methods are used, whereby a value of the top mass (and two more quantities related to the neutrinos) is assumed, and the probability of the observed topology is calculated. These results are published, and so here we compare the uncertainties on the top mass from different sources for CDF and DØ: for the lepton+jets channel in Table 2, and for the dilepton channel in Table 3 (these tables represent a huge amount of work by both collaborations). The dominant overall uncertainty is in the jet energy scale.

TABLE 2. Summary of the CDF and DØ measurement of the top quark mass in the Lepton+Jets channel.

Lepton + Jets Analyses		
Quantity	CDF	DØ
Integrated Luminosity	109	125 (?)
Total Events Fit	76	77
Tagged Events	34	5
Dble-tagged Events	5	0
< Est. $t\bar{t}$ Evts>	45	24-32
$e/\mu/e_{tag}/\mu_{tag}$	21/21/16/18	35/37/2/3
Top Mass and Uncertainties (in GeV)		
Final Fit Mass	175.9 ± 6.9	173.3 ± 7.9
Stat. Uncertainty	4.8 GeV	5.6 GeV
Tot. Syst. Uncertainty	4.9 GeV	5.5 GeV
Quoted Systematic Uncertainties (in GeV)		
Jet Energy Scale	–	4.0
Generator: '$t\bar{t}$ signal'	–	1.9
Generator: 'Vecbos Flavors'	–	2.5
Noise/Mult. Int	–	1.3
MC Stat	–	0.85
LB/NN Diff	–	0.8
Likelihood fit	–	1.0
Jet energy scale/soft glue	4.4	–
Initial state rad.	1.4	–
Final state rad.	1.1	–
Bkgd shape	1.3	–
b-tag bias	0.4	–
Pdf's	0.3	–
MC generators	0.1	–

7. The Top Mass – W Mass plane

The W mass gets radiative corrections of order $ln(m_H/m_W)$ and $(m_T/m_W)^2$ from the Higgs mass and top quark masses, respectively. Measuring the three quantities α_{em}, G_F, and m_Z constrains the two electroweak couplings g, $g\prime$, and the mixing angle $sin(\theta_W)$. Measuring m_W and m_{top} then constrains the Higgs mass, as shown graphically in Figure 7. At present the Tevatron results are only partial, with the DØ and CDF numbers being preliminary, and the CDF electron channel not yet finished. In addition

TABLE 3. Summary of the CDF and DØ measurement of the top quark mass in the Dilepton channel.

Dilepton (e, μ) Analyses		
Quantity	CDF	DØ
Integrated Luminosity	109	125 (?)
Total Events Fit	8	6
$e\mu/ee/\mu_\mu$	7/0/1	3/2/1
Tagged Events	3 (2 SVX+SLT, 1 SVX)	1 (SLT)
< Est. $t\bar{t}$ Evts>	6.7	4.5
Top Mass and Uncertainties (in GeV)		
Final Fit Mass	$167.4^{+11.7}_{-10.9}$	168.4 ± 12.8
Stat. Uncertainty	$^{+10.7}_{-9.8}$ GeV	12.3 GeV
Tot. Syst. Uncertainty	4.8 GeV	3.7 GeV
Quoted Systematic Uncertainties (in GeV)		
Jet Energy Scale	3.8	2.4
Signal Model	–	1.8
Multiple Int.	–	1.3
Likelihood fit	–	1.3
Bkgd Model	–	1.2
Jet energy scale	3.8	–
Final state rad.	2.4	–
Initial state rad.	1.2	–
Bkgd shape	1.3	–
MC generators	0.6	–
MC statistics	0.7	–

the LEP measurements will improve substantially. However one can already see that the Higgs is expected to be light, and that with improved precision on the W mass the improved measurements of the top mass in Run II will tightly constrain the SM Higgs mass.

8. Associated Higgs Production

While the cross-section for gluon-gluon fusion into a Higgs is higher than the associated production of a W and a Higgs by a factor of ≈ 3 for a 100 GeV Higgs (≈ 2 for a 200 GeV Higgs)[17], the decay products of $b\bar{b}$ or $\tau\bar{\tau}$ are difficult to trigger on and to separate from the QCD two-jet background (this is easy to see- we can't do the Z^0, with its much higher cross-section).

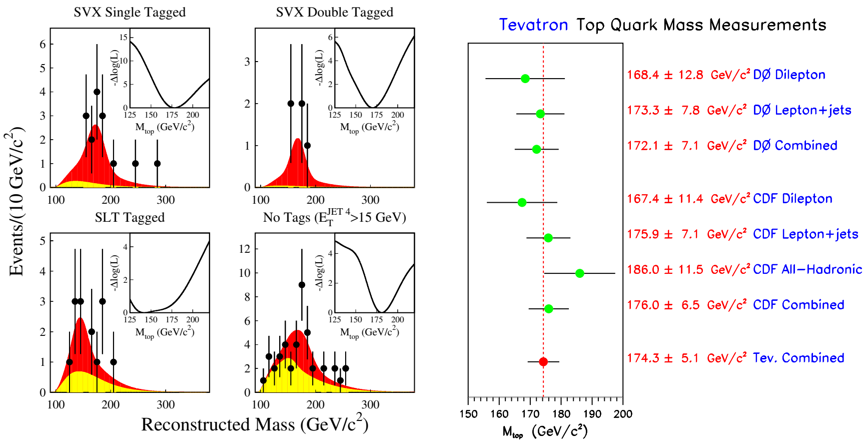

Figure 6. Left: The reconstructed top mass compared to Monte Carlo for the four subsamples of the top sample; the insets give the likelyhood versus fit mass. Right: A summary of the CDF and DØ top mass measurements (another 'too good to be true' plot.)

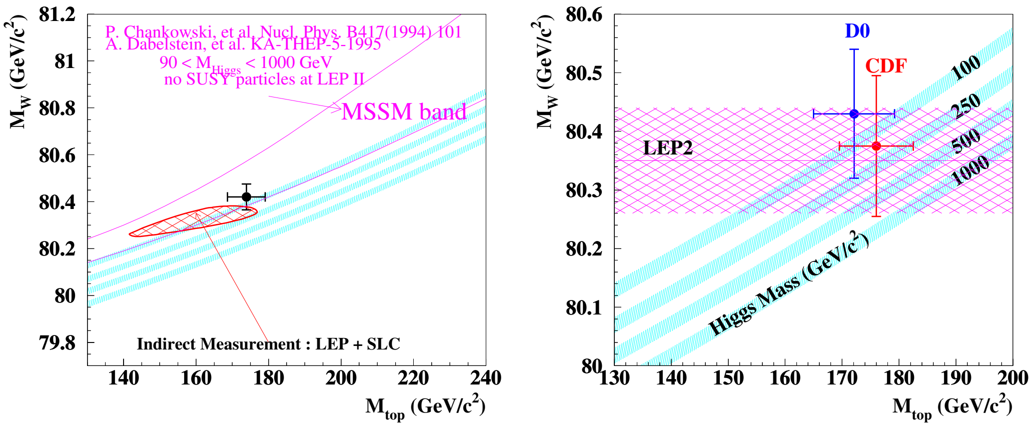

Figure 7. Left: The M_W M_{top} plane showing the world average direct measurements (point) and the constraints from precision measurements from LEP and SLAC. The hatched bands represent the allowed regions for values of the Higgs mass of 100 - 1000 GeV, as labelled on the right-hand plot. Right: A similar plot, with the LEP, CDF, and DØ mass measurements explicitly shown.

At the Tevatron one instead looks at WH and ZH production, with the vector boson decaying either leptonically or hadronically (two jets). Figure 8a shows the status of searches from both CDF and DØ; the SM cross-section versus Higgs mass is also shown, and it should be noted how small it is.

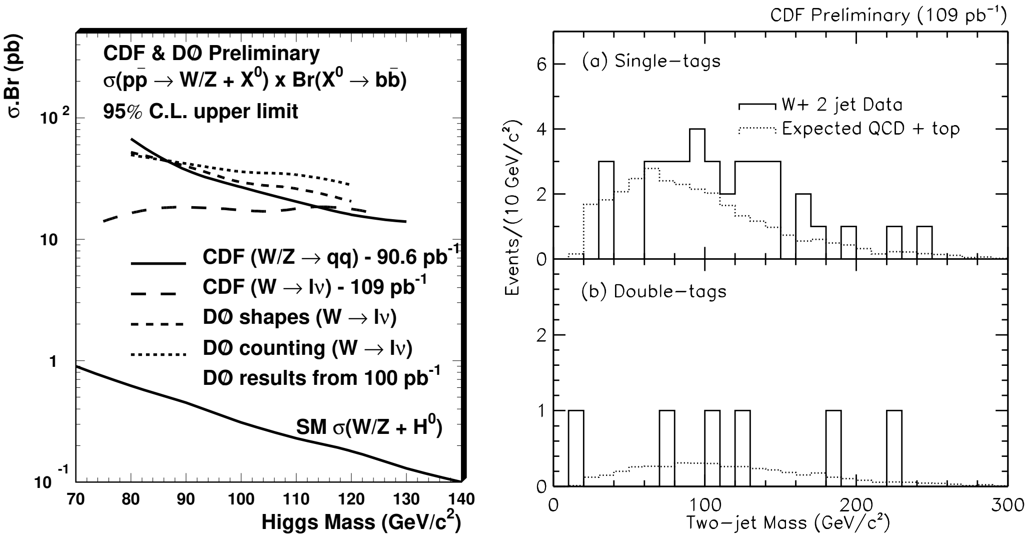

Figure 8. Left: A summary of the CDF and DØ limits on associated Higgs production, compared to the SM cross-section. Right: The dijet spectra for Wjj events with one jet tagged (top) or two jets tagged (bottom).

Figure 8b shows, as an example of the background level, the dijet spectrum for events with a $W^{\pm} \rightarrow l^{\pm}\nu$ decay, and two jets, with either one jet (upper plot[18]) or two jets (lower plot) tagged as b-jets. Detailed estimates of the reach in Run II are in progress; however, from these plots alone one can see that with a factor of 20 more data and a factor of 2-4 from better detectors it is highly unlikely that with 2 fb^{-1}one can reach a mass of 130 GeV, the theoretical upper limit.

9. Searching for New Physics: the Evolution of Signatures

The range and complexity of signatures of SUSY have greatly increased as we have learned to use our detectors. Table 4 gives the signatures used in SUSY searches in Run0 (the 1988-89 Run of the Tevatron). In contrast, the signatures looked at in Run I are given in Table 5. The use of heavy-flavor tagging, and a breaking away from the narrow list of SUGRA signatures toward signature-driven searches are evident.

10. Some SUSY Searches: the Stop and Squark/Gluino Searches

I will select just a few of the many searches for SUSY as examples of the techniques and problems. The lectures went through several in real detail; a more complete summary than is given here is available in Refs. [1, 2].

TABLE 4. Published SUSY searches by year from Tevatron Run 0.

Year	Title	Signature	Reference
1989	Limits on Masses of Supersym. Particles..	$\not{E}_t + \geq 1$jets	PRL62, 1825
1990	Search for a Light Higgs..	$We\nu$+2 trks	PRD41, 1717
1991	No publications		
1992	Search for Squarks and Gluinos..	$\not{E}_t + \geq 2$ jets	PRL69, 3439
1993	No publications		
1994	Search for Top Quark Decay to Chgd Higgs..	$\tau + \not{E}_t$+jets	PRL72, 1997
1995	Search for Sqks and Gluinos via Rad. Dec..	$\gamma\gamma + \not{E}_t$	PRL75, 1017

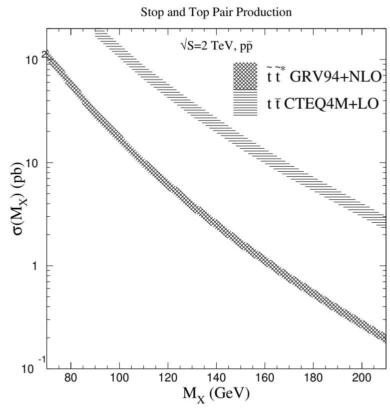

Stop Production Modes and Signatures

$\tilde{t}$ Decay Mode	Direct Production	Top Decay
$b\tilde{\chi}_1^+$	$\tilde{t} \to b\tilde{\chi}_1^+, \tilde{\chi}_1^+ \to W^+\tilde{\chi}_1^0$ $\bar{\tilde{t}} \to \bar{b}\tilde{\chi}_1^-, \tilde{\chi}_1^- \to W^-\tilde{\chi}_1^0$	$t \to \tilde{t}\tilde{\chi}_1^0, \tilde{t} \to b\tilde{\chi}_1^+$ $\bar{t} \to \bar{b}W^-$
Signature	2 b jets, 2 W's, $\not{E}_t$	2 b jets, 2 W's, $\not{E}_t$
Selection	b,l,$\not{E}_t$	
$bl\tilde{\nu} - or - b\nu\tilde{l}$	$\tilde{t} \to bl\nu\tilde{\chi}_1^0$ $\bar{\tilde{t}} \to \bar{b}l\nu\tilde{\chi}_1^0$	$t \to \tilde{t}\tilde{\chi}_1^0, \tilde{t} \to bl\nu\tilde{\chi}_1^0$ $\bar{t} \to \bar{b}W^-$
Signature	2 b jets, 2l, $\not{E}_t$	2 b jets, l, W's, $\not{E}_t$
Selection	l,l,j,$\not{E}_t$	
$c\tilde{\chi}_1^0$	$\tilde{t} \to c\tilde{\chi}_1^0$ $\bar{\tilde{t}} \to \bar{c}\tilde{\chi}_1^0$	$t \to \tilde{t}\tilde{\chi}_1^0, \tilde{t} \to c\tilde{\chi}_1^0$ $\bar{t} \to \bar{b}W^-$
Signature	2 c jets, $\not{E}_t$	b jet, c jet, W, $\not{E}_t$
Selection	c,c,$\not{E}_t$	

Figure 9. Left: The stop quark pair production cross-section versus stop mass, compared to the top quark cross-section for a 'top quark' of the same mass. Right: A table of the signatures from stop decay, including stop production in top decay.

10.1. STOP DECAYS

One of the two stop quarks is most likely the lightest sparticle that is produced via the strong interaction, as the splitting between the two mass eigenstates is expected to be proportional to the corresponding fermion mass (in this case the mass of the top quark). Because the production is via QCD, the cross-section is well predicted, and depends only on the stop mass as shown in Figure 9a[19] Also shown is the top-quark cross-section, which is larger by about a factor of 10 due to threshold factors and spin state counting. The stop decay signature, however, is model-dependent. Figure 9b gives the possible signatures, including those coming from top decay into stop.

Figure 10a shows the results of a CDF search for $\tilde{t} \to c\tilde{\chi}^0$, resulting in a final state with two charm quarks and $\not{E}_{\rm T}$[15] (I have chosen this search as

TABLE 5. A compilation of Run I Tevatron SUSY searches. The symbol b denotes an additional b–tagged jet. The integrated luminosity is indicated in italics for Run I-A. (Updated from Carena, Culbertson, Eno, Mrenna *et al.*. hep-ex/9712022).

Sparticle	**Signature**	$\int \mathcal{L}dt$ **(pb^{-1})** **CDF**	**DØ**
Charginos	$\not\!\!E_t$+trileptons	107	*13*+ 95
and	$\gamma\gamma+\not\!\!E_t$,b,τ, or jets	85	
Neutralinos	$\gamma\gamma+\not\!\!E_t$	106	
Squarks	$\not\!\!E_t+\geq$3,4 jets	*19*	*14*
and	$\not\!\!E_t+\geq$3 jets		79
Gluinos	dileptons + $\geq$2 jets	*19*	
	$\not\!\!E_t$+dileptons+ $\geq$2 jets	81	
	$\not\!\!E_t$+dileptons		92.9
Stop	$\not\!\!E_t+\ell+\geq$2 jets+b		90
	$\not\!\!E_t+\ell+\geq$3 jets+b	110	
	dilepton+jets		74.5
	$\not\!\!E_t$+2 jets		*7*
	$\not\!\!E_t+c\bar{c}$	90	
	$\not\!\!E_t+\gamma+b$	85	
Sleptons	$\gamma\gamma\ \not\!\!E_t$		106
Charged Higgs	dileptons + $\not\!\!E_t$	*19*	
	τ+2 jets+$\not\!\!E_t$	*19*	
	$\tau+b+\not\!\!E_t+(\ell,\tau,$jet)	91	
	$\tau+b+\not\!\!E_t+(\ell,\tau,$jet)		125
Neutral Higgs	$WH\rightarrow\ell+\not\!\!E_t+b$+jet	109	
	$WH\rightarrow\ell+\not\!\!E_t+b$+jet		100
	$WH,ZH\rightarrow\gamma\gamma$+2 jets		101
	$ZH\rightarrow b$+jet+$\not\!\!E_t$		*20*
	$WH,ZH\rightarrow$ 2 jets+2 b's	91	
R violating	dilepton+$\geq$ 2 jets	105	
Charged LSP	slow, long–lived particle	90	

an example out of many stop searches because of the flavor identification.) The signal is expected to appear largely in the two-jet bin for events with missing Et. Figure 10b shows the exclusion region in the $\tilde{t}-\tilde{\chi}^0$ mass plane.

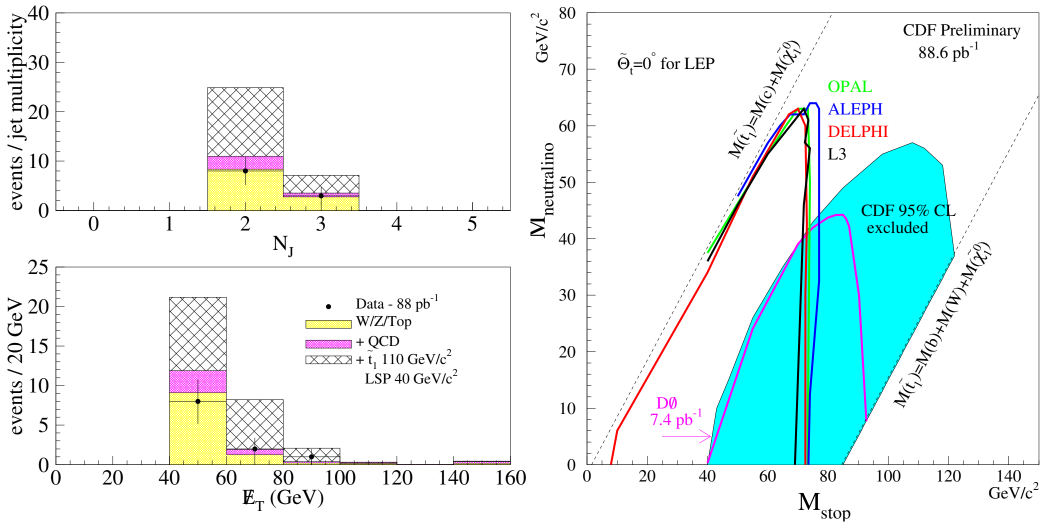

Figure 10. Left: The spectra in the number of jets (top) and $\not\!\!E_T$ (bottom) observed in the CDF stop search. The hatched area is the expected signal for a 110 GeV stop squark, with a neutralino mass of 40 GeV. Right: The excluded region in the stop mass versus neutralino mass plane.

10.2. SQUARK AND GLUINO DECAYS

Squarks and gluinos are also produced strongly, and hence with known cross-sections versus mass (see Figure 11a[19]). Both CDF and DØ have looked at the signature "$\not\!\!E_t$+ jets' that results from Gluino $\rightarrow$ Squark+quark, Squark $\rightarrow$ quark+Chargino/Neutralino; or Squark $\rightarrow$ Gluino+quark, Gluino $\rightarrow$ quark+antiquark+ Chargino/Neutralino (note the gluino is a Majorana particle, so one can get same sign dileptons from the Chargino/Neutralino decays as well as jets).

Let us take the DØ $\not\!\!E_t$ +Jets analysis as an example[1]. The signature selected is $\geq$ 3 jets $E_T > 25$ GeV, Jet1 > 115, Σ Jets$_{2-N}$ ($E_T > 15$) $>$ 100-250, and $\not\!\!E_t > 100 - 250$ GeV. They find 15 events in 79 pb^{-1}, where 9$\pm$ 4 are expected. The typical efficiency for a signal in a SUGRA model is 8% for $m_0 = m_{1/2} = 100$ GeV.

Figure 11 shows the exclusion plot for a SUGRA model with tan$\beta = 2$, $A_0 = 0$, and $\mu < 0$. Plots like these, while pretty, are hard to understand without a great deal of accompanying information from the authors. For example, the 'nose' in the excluded area comes from the fact that for $M_{\tilde{Q}} \simeq M_{\tilde{g}}$ the $\tilde{g}\tilde{g}$ cross section is supplemented by the $\tilde{g}\tilde{Q}$ cross section. In addition, what we call the 'soup' (all the cascade decays which depend strongly on the parameters across the space) is turned on, and the stop squark is lighter

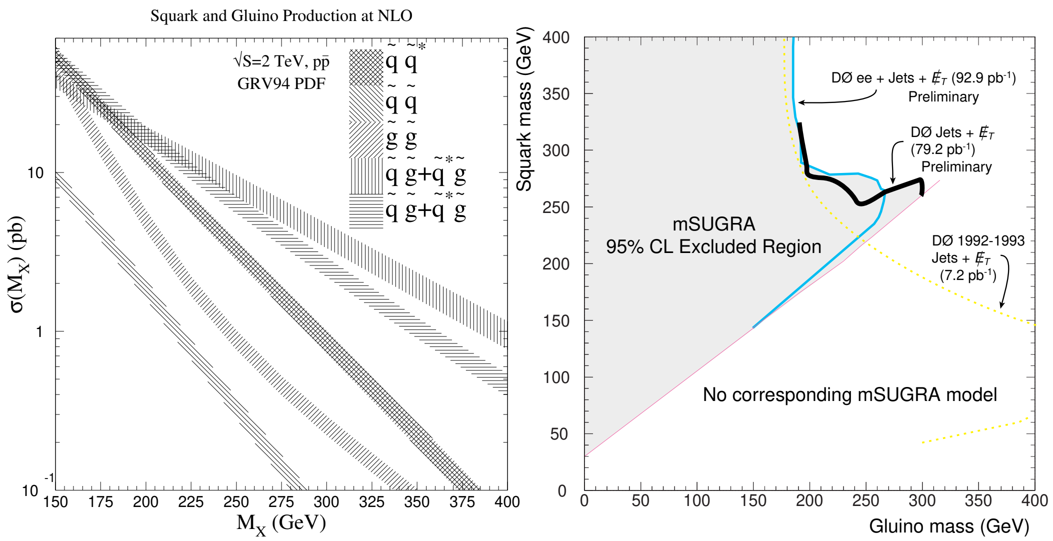

Figure 11. Left: The squark and gluino cross-sections at 2 TeV (from Spira). Right: The DØ exclusion plot in the squark and gluino mass plane in minimal SUGRA, with $tan(\beta) = 2$, etc.(see Ref. 1)

than the other squarks ($\sim$ 170 GeV, as $(A_0 \neq \mu/tan(\beta))$. The limit plot itself is very parameter dependent. Lastly, CDF and DØ have generated similar plots, but with slightly different assumptions and parameter values, but not provided enough information to compare or combine them. The limit plots have less value long-term, I believe, than a clear description of the cross-section limits on the signatures, which then can be used to set limits on models past and future.

10.3. SUSY SEARCHES WITH PHOTONS

The analysis by CDF of a very strange event with two photons and two electrons (objects that pass the standard electron cuts used in the top search, e.g.; see the discussion of subtleties in Section 4.1) sparked both theoretical interest and a round of searches for signatures involving photons. Both DØ[20] and CDF[16] have searched for events with two photons and $\not{E}_T$; DØ has also made a search for one photon with two jets; CDF has searched for one photon + b-jet with and without $\not{E}_T$. Searches in other channels are still going on; here we show the final results from the CDF search for additional two-photon events as an illustration. The analysis is described in great detail in Ref. [16].

Figure 12a shows the missing Et spectrum for events selected with two high-E_T photons ($E_T > 25$ GeV) in the central region; the one entry way

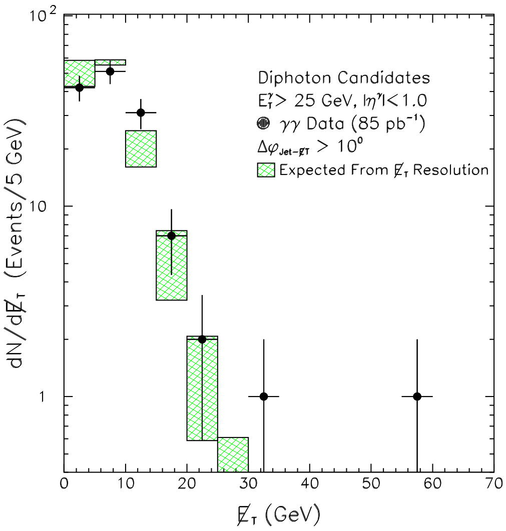

$E_T^{\gamma} > 12$ GeV Threshold		
Signature (Object)	Obs.	Expected
$\not{E}_T > 35$ GeV, $\lvert\Delta\phi_{\not{E}_T-\mathrm{jet}}\rvert > 10^{\circ}$	1	0.5 ± 0.1
$N_{\mathrm{jet}} \geq 4$, $E_T^{\mathrm{jet}} > 10$ GeV, $\lvert\eta^{\mathrm{jet}}\rvert < 2.0$	2	1.6 ± 0.4
Central e or μ, $E_T^{e \text{ or } \mu} > 25$ GeV	3	0.3 ± 0.1
Central τ, $E_T^{\tau} > 25$ GeV	1	0.2 ± 0.1
b-tag, $E_T^{b} > 25$ GeV	2	1.3 ± 0.7
Central γ, $E_T^{\gamma_3} > 25$ GeV	0	0.1 ± 0.1
$E_T^{\gamma} > 25$ GeV Threshold		
Object	Obs.	Exp.
$\not{E}_T > 25$ GeV, $\lvert\Delta\phi_{\not{E}_T-\mathrm{jet}}\rvert > 10^{\circ}$	2	0.5 ± 0.1
$N_{\mathrm{Jet}} \geq 3$, $E_T^{\mathrm{Jet}} > 10$ GeV, $\lvert\eta^{\mathrm{Jet}}\rvert < 2.0$	0	1.7 ± 1.5
Central e or μ, $E_T^{e \text{ or } \mu} > 25$ GeV	1	0.1 ± 0.1
Central τ, $E_T^{\tau} > 25$ GeV	0	0.03 ± 0.03
b-tag, $E_T^{b} > 25$ GeV	0	0.1 ± 0.1
Central γ, $E_T^{\gamma_3} > 25$ GeV	0	0.01 ± 0.01

Number of observed and expected $\gamma\gamma$ events with additional objects in 85 pb^{-1}

Figure 12. Left: The spectrum from CDF in $\not{E}_T$ for diphoton events (points) compared to that in Z^0 events (hatched boxes); the point at large $\not{E}_T$ is the '$ee\gamma\gamma\not{E}_t$' event. Right: A table of signatures, the SM expectations, and the number of events observed in the CDF diphoton search.

out on the tail is the '$ee\gamma\gamma\not{E}_t$' event. The background shape in $\not{E}_T$ is derived from $\not{E}_T$ in the ever-helpful Z^0 events. Figure 12b is a table of other interesting signatures, the standard model expectations, and the number of events found. The '$ee\gamma\gamma\not{E}_t$' remains as the only unusual event in this sample; while interesting, not much can be made of one event beyond speculation, and looking in other channels.

11. Signature-based Searches versus Model-Driven Searches

Many of the searches for new particles at the Tevatron described in Tables 4 and 5 have resulted in limits on masses of SUSY particles within the 5-parameter SUGRA framework, or variations of the above. This has the benefit of allowing the extraction of limits that would not be possible in any larger parameter space, but also has some clear drawbacks. An alternative (not necessarily exclusive, but complementary) is for experimentalists to work on 'signature-based' searches, and to present the limits in terms of cross-section limits for contributions beyond those expected from the Standard Model. I've met a lot of resistance to this, but this is in fact old-fashioned good science: we have an '*a priori*' hypothesis, the Standard Model, whose predictions we are testing. The signatures of *a priori* interest include final states with gauge bosons (new states are likely to decay via cascade decays through the gauge bosons; pairs of new states will give pairs of bosons), and states with the third generation particles the τ, bottom, and top. Examples of specific signatures are 2 leptons +X, photon + lepton, photon + b, multiple leptons, ... Table 11 lists some advantages and disadvantages of the two complementary approaches. Obviously both

TABLE 6. A 'score-card' on the advantages and disadvantages of signature-driven searches for SUSY versus model-driven.

Score	Signature-Driven	Model-Driven
+	Look in a large number of channels with *a priori* cuts- compare to SM	Look where theorists tell you to
+	Eyes open to the unexpected (rare events, e.g. the tau, J/ψ,	Eyes tend to be focussed on models: tight cuts
−	A priori criteria may make one avoid difficult channels or detailed analyses	Hot topics focus a lot of interest on difficult channels (e.g. $\sin(2\beta)$)
+	Develops (promotes) general tools for many channels	Can develop general tools, but often doesn't
−	Tends not to be optimized for specific channels	Optimized for better discovery potential in a few channels
+	Forward-looking: limits on cross-sections applicable to later theory	Results age rapidly as theory moves

have merit, and we need to have both. The Tevatron experiments, having been heavy on the SUGRA limits, are now moving toward signature-based searches to limit a much wider variety of models and possibilities.

12. Conclusions and Prospects

In Run II the CDF and DØ detectors will be much more powerful, if all goes as planned, with much-improved vertex detectors and tracking systems allowing much higher efficiencies for flavor-tagging. Another critical part of my optimism for a major discovery next run is that the cross-sections for sparticle production are typically at least 10's to 100's of femtobarns for masses in the range of 100- 150 GeV for gauginos and many hundreds of GeV for squarks and gluinos. With a factor of 20 in integrated luminosity ($2\,\mathrm{fb}^{-1}$), and better discrimination among signatures we will, I predict, find new physics beyond the Standard Model. Figure 13 shows the history of integrated luminosity at high-energy hadron colliders; the W and Z were discovered when the luminosity reached SM electroweak cross-sections; the top quark was discovered also when several hundred pairs had been produced. This is going to be fun.

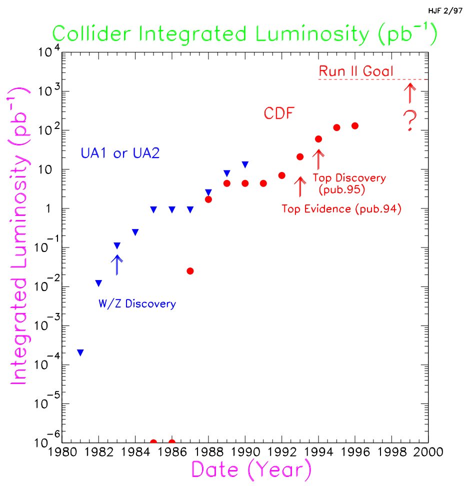

Figure 13. The integrated luminosity versus time at $\bar{p}p$ colliders.

13. Acknowledgements

I would like to thank Pierre Bientruy and Gerard Smadja for running a wonderfully organized and exciting school, the staff, who are marvelous, and the many students with whom I had discussions. I thank Regina Demina, Mark Lancaster, Young-Kee Kim, Rob Roser, Michael Spira, and Weiming Yao for supplying figures. I thank Amy Connolly, Regina Demina, and Olga Dubois for reading the manuscript.

References

1. Carena,M., Culbertson, R.L., Eno, S., Frisch, H.J.,and Mrenna, S. (1998) Searches for Supersymmetric Particles at the Tevatron Collider, to be published in *Reviews of Modern Physics*, hep-ex/9712022.
2. Carena,M., Culbertson, R.L., Eno, S., Frisch, H.J.,and Mrenna, S. (1998) The Search for Supersymmetry at the Tevatron Collider in *Perspectives in Supersymmetry*, G.L. Kane, ed., World Scientific.: QC174.17.S9 P47, hep-ex/9802006
3. The Main Ring has been replaced by a new accelerator, the Main Injector, in a separate tunnel. For more information on the accelerator complex, including pictures, Fermilab has introductory material at http://www.fnal.gov/pub/accel_tour.html.
4. The numbers are from the Fermilab Accelerator Division at http://www-fermi3.fnal.gov/luminosity.html. For details about the Tevatron upgrade, see the very complete description at http://www-bd.fnal.gov/lug/runII_handbook/RunII_index.html.
5. The limit is actually bytes per second and not events; many more events could be written if different formats for different kinds of events could be used.
6. Abbott, B., et.al., (1998) Phys. Rev. **D58**, 092003; http://www-d0.fnal.gov/public/wz/wmass/wmass.html.
7. Avila,C. et al., (1999) A Measurement of the Proton-antiproton Total Cross Section at $\sqrt{s} = 1.8$ TeV, *Phys.Lett.* **B445**:419-422. The CDF and DØ experiments normalize to cross-sections that are different by 4%.

8. Dittmar, M., Pauss, F., Zurcher, D., (1997) Towards a Precise Parton Luminosity Determination at the CERN LHC. *Phys.Rev.* **D56**:7284-7290, hep-ex/9705004
9. Rossi, B., *High-energy Particles*, New York: Prentice-Hall, 1952.
10. Abe, F., et al., (1994) Evidence for top quark production in $\bar{p}p$ collisions at $\sqrt{s} = 1.8$ TeV, *Phys. Rev.* **D50**, 2966; http://www-cdf.fnal.gov/physics/pub94/pub94.html There are now a bewildering number of papers on the top quark cross-sections and mass measurements from CDF and DØ. In the interest of saving space, I have where possible referenced the most detailed discussions of techniques, which typically occur in the large Phys. Rev. D summaries. However the collaborations have provided excellent web sites with links to the papers: for references to the CDF papers on the specific measurements of the properties of the top quark and the W, see http://www-cdf.fnal.gov/physics/physics.html; for DØ, see http://www-d0.fnal.gov/www_buffer/pub/publications.html.
11. Abachi, S., et al., (1995), Top Quark Search with the DØ 1992-1993 Data Sample *Phys. Rev.* **D52** 4877; http://www-d0.fnal.gov/www_buffer/pub/publications.html
12. Abe, F., et al., (1994) The $\mu\tau$ and $e\tau$ Decays of Top Quark Pairs Produced in $\bar{p}p$ Collisions at $\sqrt{s} = 1.8$ TeV, *Phys. Rev. Lett.* **79**, 3585; http://www-cdf.fnal.gov/physics/pub97/pub97.html
13. Hohlmann, M. (1997), Observation of Top Quark Decays in the Dilepton Decay Channel Using Electrons, Muons, and Taus, Ph.D thesis (Univ. of Chicago); http://hep.uchicago.edu/cdf/theses.html
14. Abbott, B., et al., (1999), Determination of the Absolute Jet Energy Scale in the D0 Calorimeters. *Nucl. Instr. and Meth.* **A424**, 352; hep-ex/9805009.
15. Holck, C., Search for scalar top, Contributed to 29th International Conference on High-Energy Physics (ICHEP 98), Vancouver, Canada, 23-30 Jul 1998, FERMILAB-CONF-98-208-E.
16. Abe, F., et al., Searches for New Physics in Diphoton Events in $\bar{p}p$ Collisions at $\sqrt{s} = 1.8$ TeV, *Phys. Rev. Lett.* **81**, 1791 (1998); Toback, D., (1998), Ph.D thesis (Univ. of Chicago); http://hep.uchicago.edu/cdf/theses.html
17. Stange, A., Marciano, W., and Willenbrock, S. (1994) *Phys. Rev.* **D49**, 2.
18. As an historical aside, these are the data that caused the widely-spread rumor of a 'bump' in $b\bar{b}$ at 110 GeV.
19. M. Spira, private communication.
20. Abachi, S., et al., (1997), Search for Diphoton Events with Large Missing Transverse Energy in $\bar{p}p$ Collisions at $roots = 1.8$ TeV, *Phys. Rev. Lett.* **78** 2070 (1997), hep-ex/9612011
21. Abe, F., et al., (1998) Measurement of the Top Quark Mass, *Phys. Rev. Lett.* **80**, 2767 (note added in proof: this is superceded by: Abe, F., et al., (1999) Measurement of the Top Quark Mass with the Collider Detector at Fermilab *Phys. Rev. Lett.* **82**, 271, which also includes updated dilepton and all-hadronic mode measurements.)
22. Abachi, S., et al., (1997), Direct Measurement of the Top Quark Mass, *Phys. Rev. Lett.* **79**, 1197-1202; Abbott, B., (1998) et al., (1998), Direct Measurement of the Top Quark Mass by the DØ Collaboration, *Phys. Rev.* **D58**, 52001-1 – 52001-39
23. Abe, F., et al., (1998) Measurement of the Top Quark Mass and $t\bar{t}$ Production Cross Section from Dilepton Events at the Collider Detector at Fermilab *Phys. Rev. Lett.* **80**, 2779
24. Abbott, B., et al., (1998) Measurement of the Top Quark Mass Using Dilepton Events, *Phys. Rev. Lett.* **80**, 2063-2068
25. Abe, F., et al., (1997) First Observation of the All-Hadronic Decay of t-tbar pairs, *Phys. Rev. Lett.* **79**, 1992 (1997).